Prediction of catastrophes: An experimental model

Randall D. Peters,[1] Martine Le Berre,[2] and Yves Pomeau[3]
[1]*Department of Physics, Mercer University, Macon, Georgia, USA*
[2]*Institut des Sciences Moléculaires d'Orsay ISMO-CNRS, Université Paris-Sud, Bâtiment 210, 91405 Orsay, France*
[3]*Department of Mathematics, University of Arizona, Tucson, Arizona, USA*
(Received 6 April 2012; revised manuscript received 22 June 2012; published 16 August 2012)

Catastrophes of all kinds can be roughly defined as short-duration, large-amplitude events following and followed by long periods of "ripening." Major earthquakes surely belong to the class of "catastrophic" events. Because of the space-time scales involved, an experimental approach is often difficult, not to say impossible, however desirable it could be. Described in this article is a "laboratory" setup that yields data of a type that is amenable to theoretical methods of prediction. Observations are made of a critical slowing down in the noisy signal of a solder wire creeping under constant stress. This effect is shown to be a fair signal of the forthcoming catastrophe in two separate dynamical models. The first is an "abstract" model in which a time-dependent quantity drifts slowly but makes quick jumps from time to time. The second is a realistic physical model for the collective motion of dislocations (the Ananthakrishna set of equations for unstable creep). Hope thus exists that similar changes in the response to noise could forewarn catastrophes in other situations, where such precursor effects should manifest early enough.

DOI: 10.1103/PhysRevE.86.026207 PACS number(s): 82.40.Bj, 05.45.−a

I. INTRODUCTION

Catastrophes as defined in the abstract are related to a class of phenomena sometimes called "relaxation" oscillations. The observation of two widely separated time scales makes relaxation oscillations a good *a priori* subject of theoretical investigation, because one may suspect that their formation results from the existence of a (more or less hidden) small parameter. This gives some hope of a general theory based upon the small size of the parameter. To take an example, some major earthquakes lasting a few tens of seconds occur in the same general area about every hundred years. They thus involve a ratio of "typical" times in the neighborhood of 10^{-9}, which is a very small number. In the present study a laboratory experiment was devised which displays similar relaxation oscillations, but acting timewise on a scale that is convenient for investigation. Experimental observations are explained in light of a two-part dynamical bifurcation model of catastrophe. Comprising the local form of a physical model shown to be valid when close to the catastrophe, the striking result is as follows. In response to an external source of noise the two models (the local one and the physical one) predict fluctuations with a correlation time that increases before the catastrophe, just as is observed experimentally. The important point is that this well-known critical slowing-down phenomenon occurs significantly before the transition and could be used to forewarn it.

We study the creeping of a soft metal under constant stress. Accurate time records show that this creeping actually displays the following time-dependent noisy component. The wire typically lengthens slowly with background (nonthermal) noise, with sometimes a "large" sliding event, followed again by a noisy slow lengthening regime, etc.

Plastic deformation of solids is a complex phenomenon that is not yet fully understood [1]. It has long been observed to take place in a nonsmooth manner. Most studies have focused on the Portevin–Le Chatelier effect observed under constant-strain-rate conditions, whereas the present experiment is concerned with creep at constant stress. In both cases large steps (cyclic slips) are embedded in a noisy background. There is a general agreement that this is due to the complex dynamics of networks of dislocations whose motion is a means for the stressed solid to flow. As reported in Sec. II below, careful observations of the creep in strained Sn-Pb quasieutectic material (a solder wire) show the following: (i) On average a sample under constant stress lengthens at a constant rate. (ii) Continuous monitoring shows time-dependent fluctuations of this length superposed on its secular increase. (iii) From time to time the length jumps by steps. Afterward a noisy and steady (on average) length increase is recovered until the next jump, etc.

Explaining all this remains a challenge for the common models of creep. Nevertheless, it is of great interest because it can be seen as a laboratory model of other far less accessible phenomena such as earthquakes, where on average there is also a continuous slow sliding with random microseismic noise, interrupted by large fast sliding steps characterizing major earthquakes. We recently introduced the idea [2] that in such systems the slow-to-fast transition can be described by a saddle-node bifurcation in a dynamical system evolving slowly with time. We pointed out the interest in such a modelization, which allows one to theoretically predict the response of this dynamical system to a noise source. It was shown that the induced fluctuations drift toward low frequencies (i.e., toward large correlation times) re the transition and so could be used as a forewarning.

Here we show that the dynamical saddle-node bifurcation model is the reduced form of a set of equations, the (AK) model, previously introduced by Ananthakrishna and Sahoo [3] to describe the Portevin–Le Chatelier effect in metals or metallic alloys, which also describes the creeping effect because the solution undergoes a Hopf bifurcation by changing continuously a parameter, which leads to steps on the creep curve [4]. The saddle-node model describes fast transitions resulting from the intrinsic dynamics of the original system, which can be described locally (close to the step) as a

slowly rocking potential system. Using the AK model as well as the saddle-node reduced model we show that, with an added external source of noise, the correlation time of the fluctuations increases before the transition, following the classical scenario of slowing down at bifurcation points. As was shown long ago by Dorodnicyn [5], the same local dynamics describes the transition from slow manifold to fast transients in relaxation oscillations of dynamical models, such as the van der Pol equation in the strongly nonlinear limit. In the present experiment, by looking at the fluctuations of the length of our samples, we found this behavior near the steplike transitions, with the characteristic drift to low frequencies before the transition, as predicted by the model.

Unlike recent publications that have presented the idea [6] that precursors of earthquakes could be found in the mechanical response to external perturbations (such as the increase of the fluctuations and their slowing down near transitions) our idea goes further, by giving an order of magnitude of the precursor time. The authors of [6] do not introduce the effect of a given time dependence of the parameters and consider only systems with steady parameter values on both sides of the bifurcation. To quote Ref. [7], "The suggested approach to analytical study of any kind of catastrophes is based essentially on the solution of a stationary problem of the possibility and conditions of the unstable equilibrium state in the system in question."

In the same spirit, used time-to-failure models [8] have also been to predict the time at which the catastrophic event occurs with a given time-independent potential. There the failure occurs via an activation energy, which usually comes from a noise source, that provides a transition from one equilibrium state to another one. These models lead to a predictor time depending upon the noise strength, not upon the dynamical property of the system itself. In the present paper the avalanche occurs from internal dynamics, which induces a hidden parameter sweeping effect, and therefore the catastrophe would exist even without any external noise. The effect of noise is to modify slightly the trajectory with respect to the no-noise case; but contrary to what happens with time-to-failure models, the avalanche time does not depend statistically on the noise amplitude, which by definition is supposed to be small. Without taking into account explicitly the time dependence of the parameters sweeping the bifurcation set, it is impossible to get the time scale for predictions. As we show, this scale depends crucially on the rate of change of the parameters near the bifurcation, which may be estimated from knowledge of the ratio of the two time scales (fast and slow ones) for saddle-node models.

Many studies have been devoted to earthquake statistics [9]. They concern their frequency of occurrence, their magnitude, and other measurable parameters. This type of study can hardly be useful for prediction purposes in our sense, that is, for the occurrence of a catastrophe just prior to it. Our purpose is to rationalize possible physical changes in observable signals that could be used to forewarn the catastrophe, without trying to understand statistical properties that require the observation of many events. For example, in the experiment that we describe, even though the statistics of the time intervals between successive sliding events seems to be well characterized, it does not help us in any way to predict the occurrence of an individual slide, without first looking at the perturbations of the measured noise, as was done.

An important challenge lies in the difficulty of stating a suitable model for a given catastrophic event. Actually, there is more than one class of possible slow-to-fast transitions in dynamical systems. The dynamical saddle node can be seen as belonging to the class of systems with an equilibrium point losing stability as a parameter changes. It is not a loss of stability, but rather a loss of existence of the equilibrium point, occurring at the folding point of the slow manifold. However, slow-to-fast transition may happen without any folding of the slow manifold. As shown in [10] by exploring a very often used mathematical representation of stick-slip behavior, the Dieterich-Ruina equations, the slow-to-fast transition can originate from the finite-time singularity of the slow dynamics itself [11]. In that case, critical speed-up, or drift of fluctuations toward large frequencies, is found to replace the critical slowing-down effect. This nonlinear phenomenon is obviously outside the class of phenomena explainable by a stability analysis of equilibria of dynamical systems. We refer the interested reader to the paper on this subject [10]. In the present paper we do not consider this case, because it is clearly not the one observed in the creeping experiments. Note that at this time it is unknown whether real earthquakes (as well as other observed catastrophes) belong to the saddle-node case with a slowing down near the transition or to the finite-time singularity case with speed-up expected, or else to another type, yet to be discovered, of slow-to-fast transition.

The creeping experiment is described in Sec. II together with the striking spectral observations. In the two sections following Sec. II, we present our theoretical approach. We present in Sec. III the abstract dynamical model showing fast jumps recently introduced by two of us [2], postponing the mathematics to Appendix A. Let us present its issue. In this model, one assumes that, as a dynamical system, the jump follows a "saddle-node" bifurcation. There a pair of fixed points, one locally stable and the other locally unstable, merge and disappear as a control parameter changes. Afterward, the system moves quickly to a new equilibrium state that is at finite distance (in phase space) from previous equilibria, whence the jump. After reviewing the saddle-node bifurcation in this light, we assume that the parameter changes with time, namely, that the parameter defining the bifurcation is itself a slow function of time. When, by this change, the parameter crosses the bifurcation value, the dynamical system makes an abrupt transition and jumps "generically" from one equilibrium state to another.

In Sec. IV we show that this "abstract" model is pertinent for describing the slow-to-fast transition in the relaxation regime of a set of equations derived by Ananthakrishna and Sahoo [3] for unstable creeping, or creeping in the relaxation regime. This set of equations describes the dynamics of populations of dislocations in the unstable creeping solid. The model shows relaxation oscillations in which slow drift is interrupted by fast variations. Near the slow-to-fast transition, we show that this model reduces to the generic equation quoted above, for a certain range of parameters. Therefore it displays a typical critical slowing down in its response to external noise, in agreement with the real data reported in Sec. II. Of particular interest is the fact that, from the experimental data, one can

predict in advance a "large-slip" event. The event is preceded by a shift toward low frequencies in the random fluctuations of specimen length.

II. CREEPING EXPERIMENT

We choose a uniform "wire" that creeps under small stress at room temperature, fabricated from a much-studied material, Sn-Pb solder, alloyed to be nearly eutectic. To establish creep at virtually constant stress, let one end of the wire be fixed and at the other end establish a constant force of tension. By this means we found the length of the wire to increase on average at a constant rate. By highly accurate monitoring of this length versus time we observed a small time-dependent part with the following pattern: on a background of fluctuations, from time to time a large slip event was observed, after which the continuous lengthening with a small background noise was recovered. The observed noise is nonthermal, since thermal noise has a far too small amplitude to be relevant. It is assumed to result from rearrangement of defect structures in the polycrystalline structure of the quasieutectic, involving dislocation dynamics. We assume that this noise originates from a source that is to first order independent of the overall lengthening of the wire. This is equivalent to saying that it is due to ongoing microscale events triggered by the imposed stress, independent of the global creeping. Therefore we analyzed the response to this noise source according to the AK equations subject to an external noise (see below).

A. Apparatus

The instrument used in these experiments, which is pictured in Fig. 1, is an extensometer [12]. Young's modulus can be accurately measured with a wire specimen, by placing different size masses on the weight pan. The trace of the vertical wire holding up the boom–weight pan in Fig. 1 has been enforced (colored in black) to be visible in the image. Though not presently used, the black clamp was for the purpose of holding a power resistor that was employed to measure the specimen's thermal coefficient of expansion. To measure temperature changes, a solid state thermometer was placed down into the sample space, through the hole seen near the top knurled clamp.

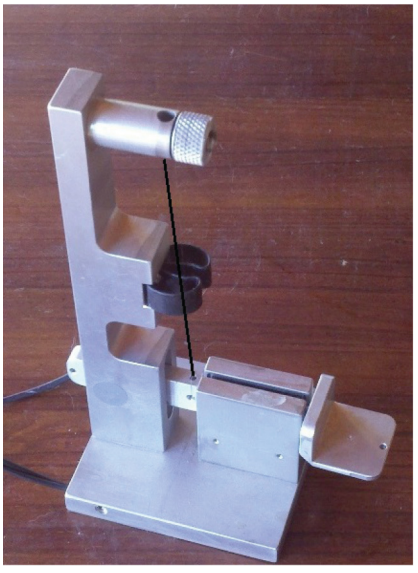

FIG. 1. (Color online) Extensometer used in the experiment.

To calibrate the instrument a 0.1-mm-diameter tungsten wire was mounted in the extensometer, and signal output level changes were recorded as various gram-mass standards were placed on the weight pan. By using the known Young's modulus for tungsten, the resulting measurements yielded a constant of $\delta\ell = 1.0$ nm per analog to digital count, for the 24-bit analog-to-digital converter employed, which is sold by Symmetric Research [15]. This constant is applicable to the data presently reported. A different measurement technique yielded essentially the same calibration constant. A He-Ne laser was used with a mirror, operating as an optical lever, to measure boom position change as different masses were placed on the pan.

Ordinary solder was chosen for the present study, which was initiated by the observation of unusual spectral features in the output from a novel seismograph [16]. The unusual low-frequency motions of the Earth's crust that were then observed to precede an earthquake [17] are readily seen by the VolksMeter. This is due to the instrument's use of a "displacement" sensor, rather than the "velocity" sensor used by conventional seismometers. It was therefore natural to consider an alloy of tin, with the expectation that its defect properties should be more like those of the Earth than is possible for a pure metal. The tin alloy for our study was ordinary soft solder (60% Sn/40% Pb), used universally in the electronics industry. Although the pure "eutectic" alloy is actually 63% Sn/37% Pb, we will nevertheless use this word to describe our specimen in the discussions that follow.

The stress level due to the load placed on the Pb-Sn wire used in the present experiments was considerably smaller than the typically 10 MPa used in usual creep studies. The present load was due solely to the weight of aluminum comprising the boom plus the empty weight pan of the extensometer. This stress value was estimated to be 0.5 MPa, based on considerations that include the distance of the wire's attachment point from the position of the (fine) roller bearing in the upright housing, which supports the boom on its end opposite the pan.

During a typical avalanche, the elongation of a 13.5-cm-long, 1.6-mm-diameter specimen would be about 30 μm. Before the avalanche, the typical lengthening velocity is 5 μm/s and typical rms fluctuations observed in the wire length (with secular term removed by high-pass filtering) would be about 50 nm.

An example of creep record (length growth versus time) is shown in Fig. 2(a). The fluctuations of the raw signal are not visible because they are much smaller than the average length variations.

B. Data analysis

To eliminate the average growth, we use a standard technique of filtering. At the exit of a high-pass single-pole filter, the filtered signal $x_n = x(n)$ is given by the recursive

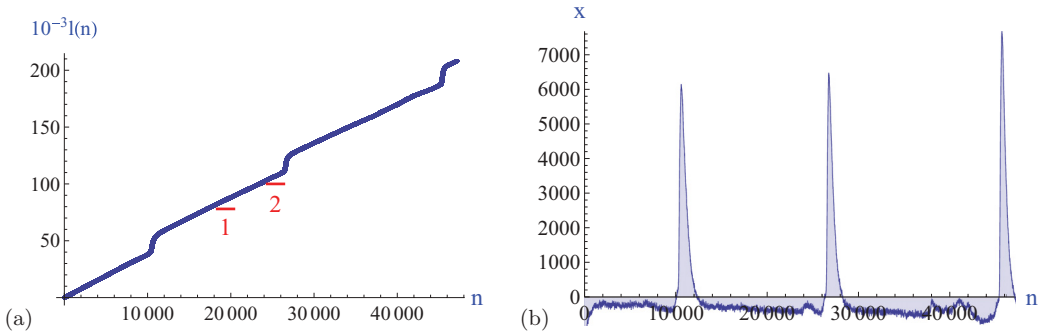

FIG. 2. (Color online) (a) Raw signal $10^{-3}\ell(n)$ of the wire elongation vs time, in digitalized sensor units. The true elongation is $\ell = \ell_n \delta\ell$, and the true time is $t = n\delta t$. (b) Filtered signal $x(n) = x_n$ at the exit of the single-pole high-pass filter defined by Eq. (1).

formula

$$x_n = \frac{1+p}{2}(\ell_n - \ell_{n-1}) + p x_{n-1}, \tag{1}$$

where $\ell_n = \ell(n)$ stands for the raw creep signal, and we set $x_1 = 0$ and $x_N = x_{N-1}$. In other words the filtered signal is the convolution product of the raw signal derivative by an exponential response function $R(t) = \exp(-2\pi f_c t)$, where f_c is the (low-frequency) corner frequency of the high-pass filter. In Eq. (1) the parameter p is given by $p = \exp(-2\pi f_c \delta t)$, where δt is the sampling time of the record, equal to $\delta t = \frac{1}{130}$ s in the experiment. By using a corner frequency $f_c = 50$ mHz, the filtered signal takes the form shown in Fig. 2(b).

In order to analyze the spectral properties of the fluctuations, and see how they evolve with time, we must consider separate sequences of a given time duration $N\delta t$. The sequences may or may not overlap, and we have tested both cases. One significant difficulty in this analysis is the proper choice for the magnitude of this time duration. The window cannot be too large, lest the spectrum becomes invariant with time. Conversely, if the window is too narrow, there will be excessive noise in the spectral (or correlation) signal. We believe the time windows have been judiciously chosen, so that there is a significant increase of the correlation time before a "burst." Such an increase of the correlation time (actually the decrease of the frequency width of the signal) was found to occur before every sliding event, giving some hope that this "critical slowing down" is pertinent for predicting the "catastrophe" before it occurs. For the present work a time duration of order 1/10 of the interval between adjacent bursts was chosen. The spectral density of the portion $[x_{n_i}, x_{n_i+N}]$ of the filtered signal corresponding to the time interval $[n_i\delta t, (n_i+N)\delta t]$, as for example one of the two intervals 1,2 marked in Fig. 2(a), can be written as

$$S_i(k) = \left| \frac{1}{\sqrt{N}} \sum_{n=n_i}^{n_i+N} x(n) \exp 2i\pi nk \right|^2. \tag{2}$$

We observe that $S_i(k)$ changes significantly during the creep process. The striking effect is the shift of the spectral density toward low frequencies in the last stage of the slow regime, i.e., just before the burst. Examples of this phenomenon are presented in Figs. 3(a) and 3(b), which show the spectra corresponding to the time intervals (1,2) marked in Fig. 2(a). The two spectra clearly differ. The spectral density in Fig. 3(a), corresponding to the first time interval marked as "1" in Fig. 2(a), displays a large number of components, whereas the spectral density in Fig. 3(b), corresponding to the time interval "2" just before the burst, is concentrated close to zero frequency. To quantify this effect, we calculate the cumulative spectrum

$$C_{S_i}(k) = \sum_{1}^{k} S_i(j), \tag{3}$$

which is a smooth curve whose asymptotic value (for $k = N$) gives the experimental variance of the fluctuations during the ith sequence considered:

$$\sigma_i^2 = C_{S_i}(N). \tag{4}$$

The shift of the spectral density toward low frequencies is visually more clear in its associated cumulative spectrum drawn in Figs. 3(c) and 3(d). We define the "low-frequency extension" of a sequence by the width w [marked on Figs. 3(c) and 3(d)] of the cumulative spectrum corresponding to 75 percent of its maximum value,

$$C_{S_i}(w) = \tfrac{3}{4} C_{S_i}(N). \tag{5}$$

Shown in Fig. 3(e) is the evolution of the spectral width w for the data of Figs. 2 and 3. The curve joins the values of w calculated for overlapping series (see the caption). A drop in w is clearly seen to occur before each burst.

The important point is that the decrease of the width before the burst is experimentally foreseeable because it occurs during a "precursor" time which is noticeably larger than the duration of a sequence, $N\delta t$. This is illustrated in Fig. 4(b), which displays an enlargement of the spectral width evolution before the burst for the data set shown in Fig. 4(a). The broken line joins the result of the data analysis, namely, the values of w_i. Because each value can be experimentally obtained at the end of each time interval $[n_i\delta t, (n_i+N)\delta t]$, the broken line joins the w_i values reported at time $(n_i+N)\delta t$.

The two following sections are devoted to theoretical models, both showing the main features of what is measured in the experiment on creeping, namely the critical slowing down of the fluctuation spectrum occurring before the sliding event. The first one is a mathematical model, which is the local form of the second one, a physical model of creeping found in the literature which consists in a set of nonlinear coupled ordinary

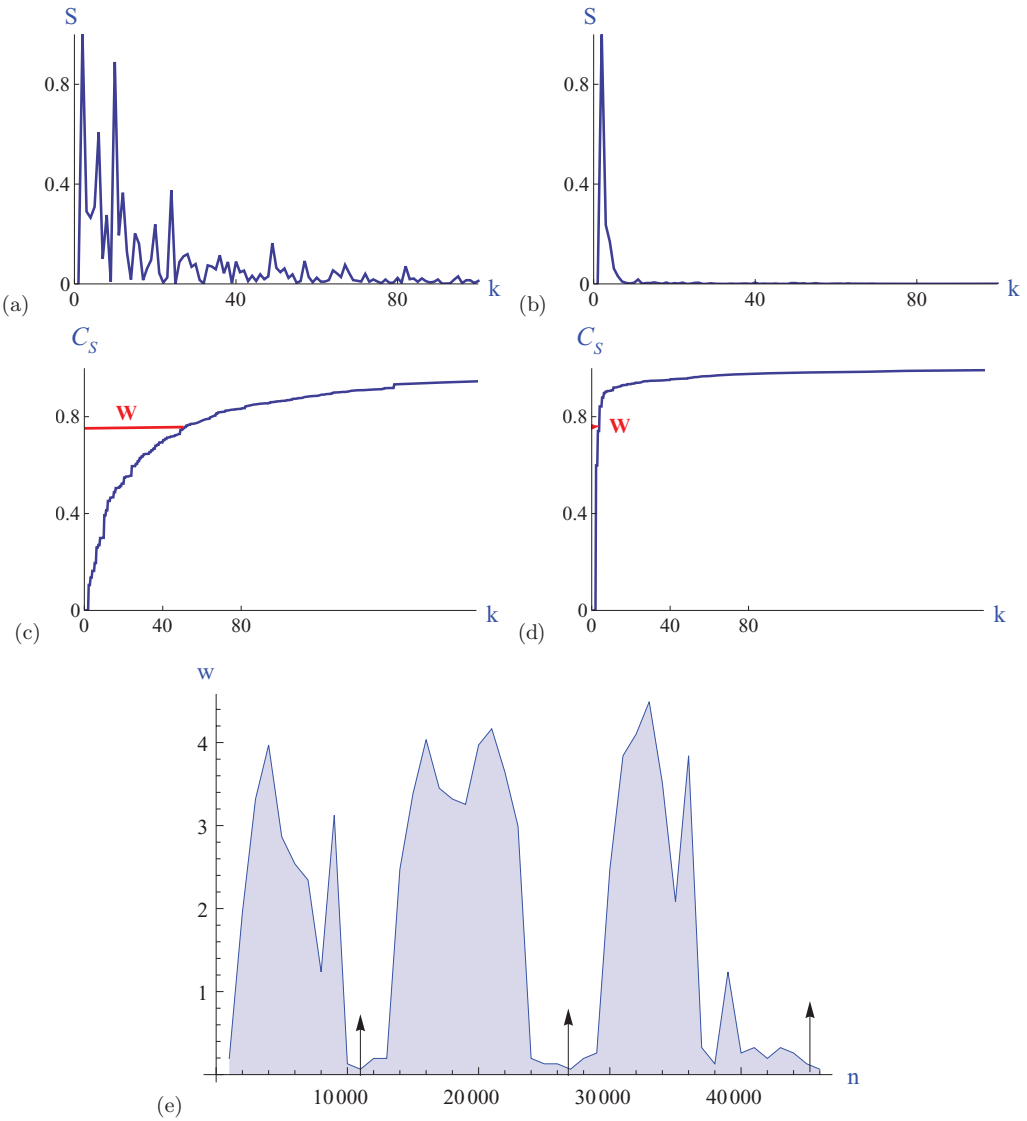

FIG. 3. (Color online) Same experimental data as in Figs. 2(a) and 2(b). Spectral density $S_{1,2}(k)$ of $x(n)$ in arbitrary units for the time intervals 1,2 marked in (a) at abscissa $18370 < n < 20370$ and $24370 < n = 26370$, respectively, each of duration is $N\delta t = 2000/130$ s. (c) and (d) Normalized cumulative spectra $C_{S_i}(k)/\sigma_i^2$, corresponding to the spectra in (a) and (b), respectively. The spectral width w defined by the relation (5) is the horizontal segment at ordinate 0.75 visible on curve (c). [A very small w_2 is barely visible on curve (d).] (e) Spectral width $w(t)$ (in a.u.) vs time $t = n\delta t$ [where w_i is the abscissa k_i such that $C_{S_i}(k_i)/\sigma^2 = 0.75$]. The three vertical arrows indicate the very beginning of the three fast steps.

differential equations, originally derived by Ananthakrishna and Sahoo [3].

III. DYNAMICAL SADDLE-NODE BIFURCATION

This section explains why a saddle-node bifurcation with a slow sweeping of the bifurcation parameter exhibits a slowing down in its response to a source of noise in a window of time extending well before the bifurcation itself. This abstract model has no direct connection with the physical phenomenon of creeping. In the section afterward, however, we explain that a model of creeping shows the same slowing down in a range of parameters, linked to a local saddle-node bifurcation.

Consider first the saddle-node bifurcation of a "gradient flow," that is, a damped dynamical system such that a coordinate $x(t)$ is a solution of the equation of motion of the form

$$\frac{dx}{dt} = -\frac{\partial V}{\partial x}. \tag{6}$$

In this equation $V(x)$ is a potential, and the dynamics tends to everywhere lower the value of $V(x)$.

The catastrophe theory of Thom and Arnol'd [18] studies how steady equilibria of equations like (6) change under smooth deformations of the potential $V(x)$. Below we consider a different kind of question, namely, what happens to the solution of Eq. (6) when the potential $V(x)$ becomes itself a slowly varying function of time, and particularly when a pair of equilibrium points disappears by a saddle-node bifurcation. Indeed this question of the sweeping across bifurcations has

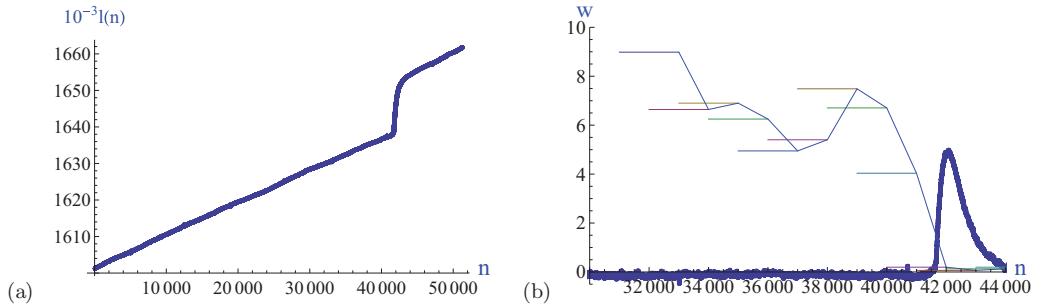

FIG. 4. (Color online) Example of data with a single avalanche. (a) Elongation $\ell(n)$ vs time, in sensor units. (b) Ten successive values of the width w_i of the cumulative spectra (before the burst) in arbitrary units, taken into the time interval $32\,000\delta t < t < 42\,000\delta t$ (or $32\,000 < n < 42\,000$). The sequences $(n_i, n_i + N)$ overlap with $N = 2000$ and $n_{i+1} - n_i = 1000$. The horizontal segments indicate the time intervals over which the width is calculated. The broken thin line joins the values of w_i taken at the end of the each sequence, at time $(n_i + N)\delta t$, to simulate an experimental observation performed in real time. The thick filled curve displays the filtered signal x_n, which indicates the avalanche time.

been already widely studied [19] with various applications in mind [where by "sweeping" we mean crossing of a transition point with a time-dependent parameter in the equation(s) of motion]. However, to the best of our knowledge the occurrence of an intermediate time scale in the case of slow sweeping has been overlooked, although we believe it to be crucial for a strategy of foretelling catastrophes in the real world.

A. Local cubic potential

Equation (6) is too general to be very helpful. However, it may describe a saddle-node bifurcation where a stable equilibrium disappears, if V depends slowly on time in a prescribed way, to become a function $V(x,t)$. Near the transition, one may use a mathematical picture which is correct for a short time around the transition if the potential $V(x,t)$ is a smooth function (see below for what happens afterward).

Assume first that $V(x)$ does not depend explicitly on time and takes the form

$$V(x) = -\left(\tfrac{1}{3}x^3 + bx\right), \tag{7}$$

with b real constant (for the moment).

For b negative $V(x)$ has two real extrema (i.e., the roots of $\frac{\partial V}{\partial x} = 0$): one, $-\sqrt{-b}$, is a stable equilibrium and the other, $\sqrt{-b}$, is an unstable equilibrium. For $b = 0$ the two equilibria merge and disappear for b positive [see Fig. 5(a)]. This is the saddle-node bifurcation. The shape of $V(x)$ near $x = 0$ and for b small is universal: for a given smooth $V(x)$ showing this saddle-node bifurcation, one can always rescale x and the external parameter to obtain the "local" problem in this form.

The extension to a time-dependent control parameter b goes as follows. If b is a smooth function of time, one can assume that $b(t)$ crosses the critical value, i.e., zero in the present case, at time zero in such a way that $b(t) = at + \cdots$ with a a nonzero constant and the dots standing for higher order terms in the Taylor expansion of $b(t)$. For t and x close to zero, after rescaling, one can represent the dynamical system (6), close to the saddle-node bifurcation, by the "universal" parameterless equation

$$\frac{dx}{dt} = x^2 + t. \tag{8}$$

Outside of the neighborhood of $x = 0$, the solution of (6) depends on other parameters defining V for finite values of x, as explained below.

Although this is not obvious from its formulation, this model is also valid for the transition from slow to fast motion in the van der Pol oscillator in the limit of large nonlinearities, as shown by Dorodnicyn [5]. We give in Appendix A a short version of the classical calculation by Dorodnicyn, showing that the "universal" equation (8) is also relevant for the slow-to-fast transitions in relaxation oscillations. It is worth mentioning that in this derivation one does not really assume that the overall motion is periodic, as it may be extended quite

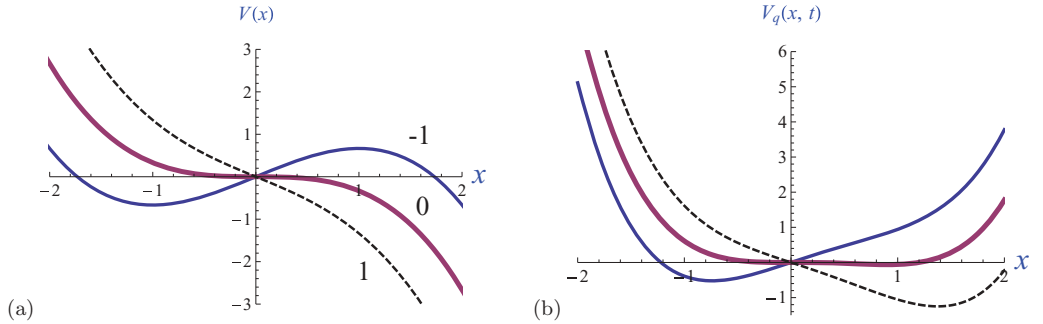

FIG. 5. (Color online) (a) Cubic and (b) quartic potentials. The parameter values $b = -1, 0, 1$ (marked next to the curves) correspond, respectively, to the blue, thick-red, and dashed-black curves.

easily to a system of many more coupled ordinary differential equations (ODEs) with only one fast variable. This shows that such large jumps are also possible in nonperiodic dynamics, because the dynamics on the slow manifold may be chaotic in between the jumps if this slow manifold has a sufficiently large number of dimensions.

The explicit solution of Eq. (8) is given in Appendix A. The solution relevant with the given condition at $t \to -\infty$ is drawn on Fig. 6(a). It diverges at time t_c, the first zero of the Airy function $Ai(-t)$, a pure number which is about $t_c \approx 2.338$ [20].

Actually the solution (A5) loses its physical meaning sometime before the singularity since the "universal" dynamical equation (8) was derived under the assumption that x remains close to zero. This local theory cannot deal with finite variations away from the critical values, and therefore we shall need to add finite-amplitude effects to limit the growth of the instability after the transition (see Sec. III B).

Now we shall focus on the slowing down near the dynamical saddle-node bifurcation described by Eq. (8). We first study the response of this dynamical system to a small external noise and then look for qualitative changes in this response which could be a signal that occurs before the transition.

Let us consider Eq. (8) with a small noise added, so that Eq. (8) is replaced by

$$\dot{x} = x^2 + t + \epsilon\xi(t), \tag{9}$$

where $\xi(t)$ is a random function of time and ϵ is a small coefficient. The numerical solutions of the stochastic equation (9) (and other stochastic equations studied below) were obtained by using Stratanovitch calculus. An example is given in Fig. 6(a), where a large-amplitude noise was chosen for clarity (to make visible the difference between the solutions with and without noise).

In the small-ϵ limit, one can solve Eq. (9) by expansion in powers of ϵ, $x(t) = x_0(t) + \epsilon x_1(t) + \cdots$. The leading order term $x_0(t)$ is the noiseless solution

$$x_0(t) = -\frac{\dot{U}(t)}{U(t)},$$

with $U(t)$ the Airy function.

The term $\epsilon x_1(t)$ is the linear response to the noise with

$$x_1(t) = \frac{1}{U^2(t)} \int_{t_0}^{t} d\tilde{t}\, \xi(\tilde{t})\, U^2(\tilde{t}). \tag{10}$$

Because $U^2(\tilde{t})$ tends rapidly to zero as $(\tilde{t})$ tends to minus infinity, one can take $t_0 = -\infty$ to get rid of the effect of the initial conditions.

We show in Appendix A that the amplitude of the fluctuations increases some time before the transition itself. As the transition approaches, the variance of the fluctuations, $\sigma(t)^2 = \langle [x(t) - x_0(t)]^2 \rangle$, increases close to the critical time t_c, because $U(t_c) = 0$.

B. Quartic potential

As the zeroth-order solution diverges at $t = t_c$, it does not make sense to describe the dynamical behavior of the fluctuations due to the external noise very close to t_c, as shown above.

As said before, this unbounded growth of the fluctuations is a consequence of the *local* cubic form of $V(x)$ when expanded near $x = 0$, in obvious contradiction with the fact that $x(t)$ tends to infinity. To suppress the divergence of $x(t)$ after the saddle-node bifurcation we add a stabilizing (positive) term to the potential $V(x)$, which becomes quartic,

$$V_q(x) = -\frac{x^3}{3} - bx + \frac{x^4}{4}, \tag{11}$$

as drawn in Fig. 5(b). Because of the growth of $V_q(x)$ at infinity, like x^4, the solution of the differential equation

$$\dot{x} = b + x^2 - x^3 \tag{12}$$

does not diverge at finite time, and it can be written in the given scaled form for any quartic potential provided the coefficient of x^4 is positive. For such a potential only one parameter remains. For $b = 0$ the dynamical system (12) is exactly at the saddle-node bifurcation, because at $b = x = 0$ both the first and second derivatives of $V_q(x)$ vanish, but not the third derivative. In contrast to the case of the pure cubic potential, this system always has, that is, for any value of b, a stable fixed point beyond the pair of fixed points collapsing at the saddle-node bifurcation. This makes it a fair candidate for describing the dynamical saddle-node bifurcation without blow-up.

As in the previous case, we shall take a time dependent b, which will be taken as $b = at$ with a a positive constant. Because of the rescaling of the cubic and quartic term, the parameter a cannot be eliminated (but another possibility would be to put a parameter in front of the cubic term). For the potential

$$V_q(x) = -\frac{x^3}{3} - a\,t\,x + \frac{x^4}{4}, \tag{13}$$

we shall analyze the solution of the dynamical equation

$$\dot{x} = at + x^2 - x^3, \tag{14}$$

tending at large negative and positive times to the equilibrium point $x = (at)^{1/3}$, t being considered as a parameter [see Fig. 6(b)]. Moreover, we consider the small-a limit, with a being related to the ratio of small to large time scales, which can be estimated from experimental data. We prove that, in this limit, there are three characteristic time intervals, depending on how close x is to zero.

The long time scale is the time lapse between successive major slips, typically of order 150–300 s in our experiments on creeping. In our model it is the time needed for the potential $V_q(x,t)$ to change significantly, to move from a pair of fixed points to a saddle-node bifurcation. Because time enters in $V_q(x,t)$ through the combination (at), the a-dimensional time needed for a change of shape of V_q is of order

$$t_{\text{creep}} \sim a^{-1}. \tag{15}$$

The short time t_{slip} is the duration of the abrupt change of slope of the function of time $x(t)$, the rising of $x(t)$ at the catastrophe time. We show in Appendix A that t_{slip} is of order unity [in units of our model equation (14)] because the local form of Eq. (14) has no explicit dependance with respect to the small parameter a. This result is confirmed by the numerics [see Figs. 6(b) and 6(c) and red curves in Fig. 7].

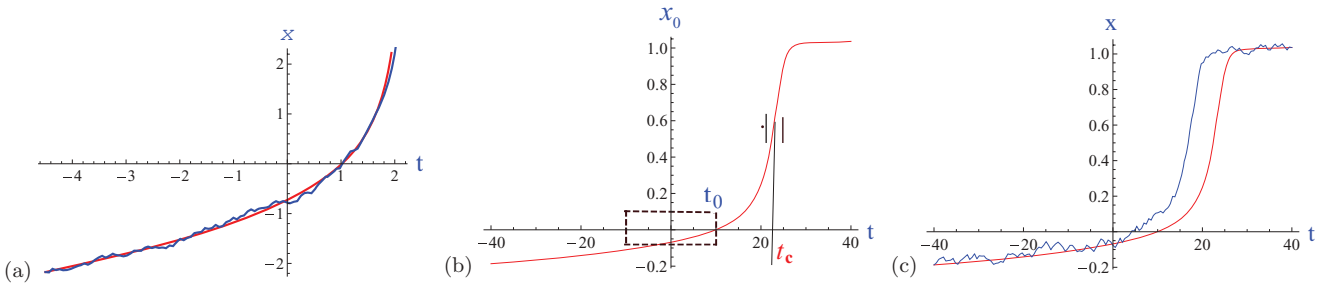

FIG. 6. (Color online) (a) solutions of Eq. (9), without noise $\epsilon = 0$ (smooth red curve) and with large-amplitude noise ($\epsilon = 1$ blue noisy curve). (b) Solution of Eq. (14) for $a = 10^{-3}$. The dashed rectangle around the origin defines the region $-t_0 < t < t_0$ and $-1/t_0 < x < 1/t_0$, with $t_0 \sim a^{-1/3}$. The critical time is $t_c(a) \sim 2.34\, t_0$. The two small vertical segments delimitate the large slope time duration, of order unity. (c) Solution of Eq. (18) without noise (smooth red curve) and with large-amplitude noise $\epsilon = 0.1$ or $\tilde{\epsilon}(a) = 1$ (blue noisy curve). The two noisy curves in (a) and (c) correspond to a single run, with a unique realization of the Langevin equation.

More precisely, defining the rising time of $x(t)$ by 1/5 of the peak width of $\dot{x}$, we have numerically

$$t_{\text{slip}} \sim 1, \tag{16}$$

independently of the value of a, for a small. In the creep experiment reported above, we had $t_{\text{slip}}^{\text{exp}} \sim 1$ s, which gives a ratio of these two time scales, $t_{\text{slip}}/t_{\text{creep}}$, as small as 10^{-2}–10^{-3}.

There is another time scale, t_0, the time interval standing before the transition, and close to it, during which the potential is very flat, while the solution has not yet jumped. During this time, x and at are much smaller than unity, and the cubic term on the right-hand side of Eq. (14) is negligible. In this range one recovers the universal equation of the dynamical saddle-node bifurcation (8) by taking $X = xa^{-1/3}$ and $T = ta^{1/3}$, with the boundary condition $X(t) \approx -\sqrt{-T}$ at T tending to minus infinity. This property concerns the rectangular domain drawn on Fig. 6(b), where x is small, $x \sim a^{1/3}$, and t extends from $t \sim -a^{-1/3}$ to $t \sim a^{-1/3}$, located before the abrupt increase. Therefore the time extension of this domain introduces the intermediate time scale

$$t_0 \sim a^{-1/3}, \tag{17}$$

which is long compared to the short time t_{slip} (of order unity) and small compared to the average time between slips, $t_{\text{creep}} = a^{-1}$. In the experiment, the value of the intermediate time scale is about 10 s by using $t_0^{\text{exp}} \sim a^{-1/3} t_{\text{slip}}^{\text{exp}}$ and $a = 10^{-3}$.

In summary, by matching the two solutions in the range $1 \ll (-\delta t) \ll a^{-1/3}$, we show that the catastrophe takes place during this time t_{slip} which is of order one, because the displacement is then of order one, compared to the small displacement of order $a^{1/3}$ taking place during time $t_0 = a^{-1/3}$ typical of the "universal" transition process.

From this understanding of the various scales in the deterministic part of the dynamical equations, we can now look at the response to noise of this system, particularly at the range of time where something like a "critical slowing down" could be observed, and which actually happens in our experiments.

With a noise source added, the dynamical equation (6) becomes

$$\dot{x} = x^2 - x^3 + at + \epsilon\xi(t). \tag{18}$$

Actually, the effective noise amplitude is not equal to ϵ close to the saddle node, as it depends on the value of the parameter a. Indeed, for $|t| \leqslant t_0$, the cubic term in Eq. (19) is negligible, and the equation reduces to

$$\dot{x} = x^2 + at + \epsilon\xi(t), \tag{19}$$

which may be written as $\frac{dX}{dT} = X^2 + T + \tilde{\epsilon}(a)\xi(t)$, by setting $X = xa^{-1/3}$, $T = ta^{1/3}$, and $\tilde{\epsilon}(a) = \epsilon a^{-2/3}$. Therefore the effective noise is larger than ϵ, by a factor of $a^{-2/3}$ in the rectangular domain of Fig. 6(b).

Let us consider now the fluctuations of the solution $x(t)$ of Eq. (19). For a small noise source, the solution may be expanded in power of ϵ as above. At first order this gives

$$\dot{x}_1 = \left[2x_0(t) - 3x_0^2(t)\right]x_1(t) + \xi(t), \tag{20}$$

whose solution is formally

$$x_1(t) = \int_{t_0}^{t} d\tilde{t}\; \xi(\tilde{t}) \exp[g(t) - g(\tilde{t})]. \tag{21}$$

In general $g(t)$ is the time integral of the second derivative of the potential, $-\frac{d^2V_q(x)}{dx^2}$, which yields with our choice of V

$$g(t) = \int_{t_0}^{t} \left[2x_0(u) - 3x_0^2(u)\right].$$

The standard deviation $\sigma_{x_1}(t)$ has to be calculated numerically. We expect it to display the same behavior as for the cubic case in the whole domain where $x(t) \ll 1$, i.e., a little before the transition and close to it, because the potential is cubic in this range. After the transition, we expect that the fluctuation decreases, because the solution without noise becomes quasi-steady. This is confirmed by the numerics: the amplitude of the fluctuations strongly increases close to the critical time $t_c(a)$ defined in Appendix A, with its maximum occurring at time $t_c(a)$, then it decreases. More precisely, the standard deviation behaves exactly as $\dot{x}_0(t)$, the red curve in Fig. 7(a), for small noise. Therefore the strong increase of the variance of the signal fluctuations cannot be used as a precursor for predicting the transition because it occurs simultaneously with the signal itself close to the transition. Note that this observation seems to contradict the currently found statement that fluctuation enhancement precedes the transition and can be used as a precursor. In the case of the saddle-node bifurcation model, we

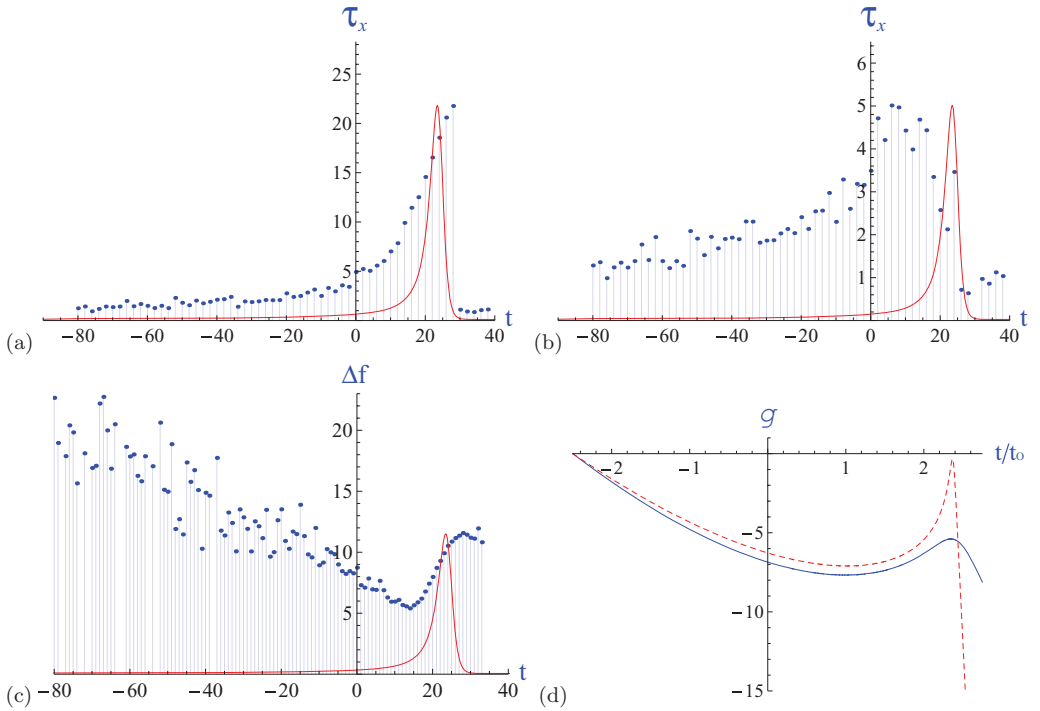

FIG. 7. (Color online) (a) and (b) Correlation time τ_x of the fluctuation $x(t) - x_0(t)$ for the saddle-node model (18) with $a = 10^{-3}$. The correlation functions are defined by Eqs. (22) and (23) for curves (a) and (b), respectively. (c) Spectral width (in a.u.) calculated with $w_g = t_0$, for $a = 10^{-3}$; the red curves display the time derivative $\dot{x}(t)$ in order to indicate the catastrophe time. (d) $g(t/t_0)$ for $a = 10^{-3}$ (solid, blue curve) and $a = 10^{-6}$ (dashed, red curve).

have indeed observed a "precursor" growth of the fluctuations, but only in the case of "large" -amplitude noise [see Fig. 6(c)]. Let us focus on the case of small amplitude noise. In this case we show below that the correlation time of the fluctuations changes much earlier than the onset of amplitude growth. This slowing down can be used to foretell the event itself, in considerable advance of its occurrence. It is seen to consistently occur in the creeping experiment described below.

Consider the case of small effective noise, where the correlation function and the spectrum of the fluctuations $[x(t) - x_0(t)]$ are well described by the correlation function and spectrum of $x_1(t)$, respectively. As noted in the previous section, the calculation of these functions requires some care because the system is not in a statistically steady state. Therefore the spectral density of the fluctuations depends on time and the correlation function $\Gamma_{x_1}(t,\tau) = \langle x_1(t-\tau)x_1(t)\rangle$ depends on both t and on the time difference τ. More precisely, the correct definition of the correlation function is actually given by

$$\Gamma_{x_1}(t,\tau) = \frac{\langle x_1(t-\tau)x_1(t)\rangle - \langle x_1(t-\tau)\rangle\langle x_1(t)\rangle}{\sigma_{x_1(t-\tau)}\sigma_{x_1(t)}}. \quad (22)$$

The latter definition of correlation is not readily accessible in experimental situations, because it requires knowledge of the time-dependent variance, which is difficult to estimate from a single sample. A more accessible tool is often used; it is given by the expression

$$\Gamma'_{x_1}(t,\tau)' = \frac{\langle x_1(t-\tau)x_1(t)\rangle - \langle x_1(t-\tau)\rangle\langle x_1(t)\rangle}{\sigma_{x_1(t)^2}}, \quad (23)$$

which coincides with the correct expression if the variance is the same at time t and $t-\tau$ only. If the variance changes noticeably during the time interval of duration τ, the latter expression is biased, since $\Gamma = \Gamma' \frac{\sigma(t)}{\sigma(t-\tau)}$. We expect such a discrepancy to manifest itself close to the catastrophe, since the variance increases there by a large amount. To illustrate this point we compare in Figs. 7(a) and 7(b) the correlation times τ_x and half-height width of the correlation functions as defined by Eqs. (22) and (23), respectively. The strong increase of the correlation time before the catastrophe is noticeably truncated when using the biased expression (23). Using the correct definition of the correlation function (22), the correlation time increases by a factor of 10 over a time interval of order t_0 before the catastrophe, while the enhancement is only about a factor of 3 when using the biased expression (23). Moreover, the enhancement is followed by a drop in the latter case. This discrepancy between the results supplied by the two definitions comes from the fact that the variance increases close to the catastrophe, as is well known [21]. Nevertheless, because both curves in Figs. 7(a) and 7(b) display well the critical slowing-down effect, which manifests as a growth of the correlation time close to the transition, we conclude that the manifestation of the slowing-down effect occurs well before the catastrophe for the spectrum than for the variance, the delay being about a few t_0 for the former, against less than t_0 for the variance.

The increase of the correlation time *before* the catastrophe is understood by looking at the formal expression (21). The second derivative of the potential vanishes at $t = t_0$, and that leads to the flatness of $g(t)$ in the time domain $0 < t < t_c(a)$,

as shown in Fig. 7(d). This time domain could therefore be identified as a "precursor time," of order a few t_0.

Now let us consider the spectrum of the fluctuations in order to compare with the experimental results. A time-dependent spectrum can be defined formally by the (real) Wigner transform

$$S_{x_1}(t,f) = \int_{-\infty}^{-\infty} d\tau \, \langle x_1(t-\tau)x_1(t)\rangle \, e^{-2i\pi f\tau}, \qquad (24)$$

which has to be modified for numerical applications, either by using a filtering procedure like the one used in the previous section or by introducing a slipping window. In this section we use the latter process. By choosing a Gaussian window function of width w_g, the numerical spectrum is given by

$$S_{x_1}(t,\nu) = \left\langle \left| \int_{t_a}^{t_b} d\tau e^{-(\frac{t-\tau}{w_g})^2} x_1(\tau) e^{-2i\pi\nu\tau} \right|^2 \right\rangle, \qquad (25)$$

where $t_{a,b}$ are the numerical integration time boundaries. This expression does not take into account the variability of the variance; therefore we expect the observed change in the spectral properties to be biased, as was the case for the correlation function Γ'.

The evolution of the spectral width Δf (half-height width) is reported in Fig. 7(c) in a range of a few times t_0 around the transition. The solution $\dot{x}_0(t)$ is drawn as a solid red line. Figure 7(c) illustrates the same effect as the correlation function Γ', but in Fourier space. The spectral width decreases noticeably from negative time of order a few t_0, until the time $t \sim 1.5t_0$, where it grows, because of the bias due to the variance increase close to the burst. The decrease of Δf corresponds to a shift of the spectrum toward low frequencies. The important result is that this shift occurs well before the transition. It occurs over a time interval of order a few t_0. This result agrees with our experiment where t_0 was estimated to be about 10 s and the decrease of the spectral width keeps on for about 30 s (see Fig. 3 where 10 s corresponds to 1300 counts on the abscissa scale). The growth of the fluctuations and their shift to lower frequencies can be understood as follows. As the transition approaches, the potential $V(x,t)$ becomes flatter and flatter, making weaker and weaker the restoring force toward equilibrium. Therefore, with a constant noise source, the amplitude of the fluctuations driven by this noise source will grow because the damping becomes less and less efficient. Moreover, the typical time scale for this damping will get increasingly larger because of the decreasing stiffness of the potential, thus favoring noise at lower and lower frequencies.

IV. ANANTHAKRISHNA MODEL

This section is devoted to an analysis of solutions of a set of equations devised for describing unstable creeping in solids. More precisely, our purpose is to show that in a range of parameters this equation exhibits a dynamical saddle-node bifurcation. As in the "abstract" model of the previous section, this bifurcation is also preceded by a slowing down of the fluctuations triggered by an external source of noise. Creeping phenomena in real materials are complex and difficult to predict quantitatively, despite decades of efforts on theoretical models. We have chosen to consider a model introduced by Ananthakrishna and Sahoo [3] for unstable creeping in strained solids. To make things simpler, we have only used its version without space dependence in the quantities involved. Note that the introduction of space variables would lead to an aperiodic creep signal more realistic than the periodic signals of the present model; however, we conjecture that it should not affect the main result of our study (the emphasis of a precursor signal over a given time interval). The AK model considered here is a set of three coupled nonlinear ordinary equations with three dimensionless parameters (a, b, and c, where the letters a and b have no connection with the same symbols used previously). The unknown time-dependent quantities are three scaled variables corresponding to three density types of dislocations, $x(t)$, $y(t)$, and $z(t)$, representing, respectively, mobile, immobile, and those with clouds of solute atoms that mimic Cottrell's idea. The model equations are

$$b\dot{x}(t) = G(x,y) = (1-a)x(t) - bx(t)^2 - x(t)y(t) + y(t), \qquad (26)$$

$$\dot{y}(t) = F(x,y,z) = bx(t)^2 - x(t)y(t) - y(t) + az(t), \qquad (27)$$

$$b\dot{z}(t) = H(z,x) = c[x(t) - z(t)], \qquad (28)$$

where the variable $x(t)$ stands for the elongation rate. As one can check, if the three variables are positive at time zero, they remain so at later times if a, b, and c are positive, as assumed. The relative elongation (or strain, or creep) $\ell(t)$ of the solder wire is the time integral of $x(t)$,

$$\ell(t) = \int_0^t x(t')dt'.$$

Solutions of Eqs. (26)–(28) have been extensively studied [1], and their shape and duration versus the parameter values are given in [4]. Recall that relaxation oscillations are depicted for small values of the parameter b only. For c larger than a certain critical value c_{cr}, depending on a and b and not written here, the solution is stable. The fixed-point coordinates are given by the expressions

$$\begin{aligned} x_s &= \frac{1-2a}{2b} \quad \text{for} \quad a < \tfrac{1}{2}, \\ x_s &= (1-a)(1+\sqrt{2}) \quad \text{for} \quad a > \tfrac{1}{2}, \\ y_s &= \frac{1}{2}, \end{aligned} \qquad (29)$$

at lowest order for the small parameter b. This fixed point becomes unstable by a Poincaré-Andronov bifurcation for small values of b, only under the condition that c becomes smaller than c_{cr}. In a large range of parameter values the limit cycle associated with the variable $x(t)$ displays relaxation oscillations characterized by slow steps and fast bursts.

In this range of b and c small, we focus on the case $c \ll b$ for two reasons. First, it allows the set of equations to be reduced to the generic saddle-node equation introduced in the previous section. Second, it leads to $x(t)$ solutions looking approximately like our experimental data [in which the strain rate $x(t)$ has to be compared with the data files labeled $y(n)$ in Sec. II]. An example of the numerical solution of Eqs. (26)–(28) is given in Fig. 8. In this case the burst amplitude drawn in Fig. 8(b) is noticeably larger than the experimental one shown

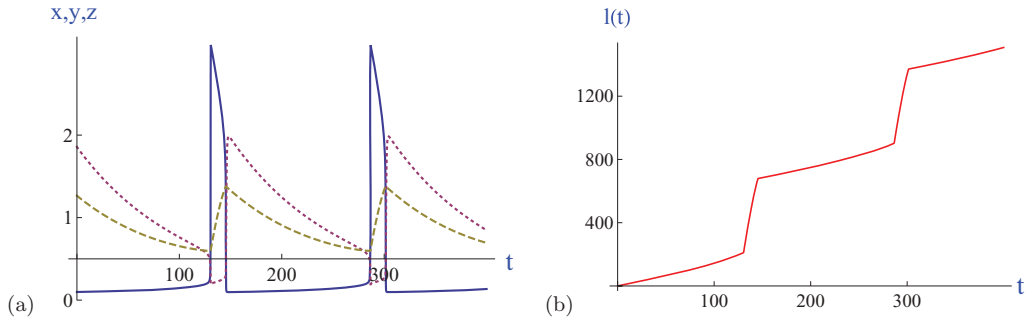

FIG. 8. (Color online) (a) Densities of mobile, immobile, and Cottrell's dislocations as a function of time, using the solution of the three-dimensional flow (20)–(28) for $a = 0.65$, $b = 4 \times 10^{-3}$, and $c = b/100$. The three curves are $0.08x(t)$ (solid), $y(t)$ (dotted),and $z(t)/5$ (dashed). (b) Creep signal $\ell(t)$.

in Fig. 2(a); nevertheless, we have chosen the parameter values for pedagogical reasons, in order to give a clear representation of the full cycle of the relaxation oscillations. Consider the evolution of the elongation rate $x(t)$ drawn as a solid line in Fig. 8(a). The limit cycle of duration $T = 180$ displays four stages. In the first step ($0 < t < 130$), the flow evolves slowly and $x(t)$ takes values of order unity. This stage is followed by a fast jump of $x(t)$ at $t \sim 130$, then by a short slow stage ($130 < t < 144$) with high values of $x(t)$, of order $1/b$, and finally followed by a fast decrease of $x(t)$ at $t \sim 144$.

The linear stability of the three-dimensional (3D) flow is derived in Appendix B. The stability along the stage preceding the fast jump is particularly informative. We show that the trajectory becomes linearly unstable shortly before the burst. Note that the time delay between the cross to zero of the linear exponents and the burst is found to be of the order of the intermediate scale t_0 for the model, which we derive analytically in the next section.

A. Normal form close to the burst

We now consider the behavior of the 3D flow in the vicinity of the burst, and we derive the normal form of the AK model close to B in order to get an estimate of the precursor time t_0. We focus on the first part of the limit cycle, preceding the burst of $x(t)$, and try to understand how the trajectory leaves the slow manifold (SM) that we define now. Because $c \ll b \ll 1$, the slow stages are described by canceling the right-hand side of Eqs. (26) and (27), which reduces the 3D flow to one-dimensional (1D) flow:

$$\begin{aligned} G(x,y) &= 0, \\ F(x,y,z) &= 0, \\ \dot{z}(t) &= \frac{c}{b}[x(t) - z(t)]. \end{aligned} \tag{30}$$

From the first equation the variable $x(t)$ is an explicit function of $y(t)$,

$$x(y) = \frac{-(y-1+a) + \sqrt{(y-1+a)^2 + 4by}}{2b}. \tag{31}$$

Inserting this expression into the second of Eqs. (30) allows us to also express the variable $z(t)$ in terms of $y(t)$:

$$z(y) = \frac{-bx(y)^2 + y[x(y)+1]}{a}. \tag{32}$$

In phase space (z,y) expression (32) defines the slow manifold, which is illustrated in Fig. 9 (red curve). On the positive slope parts of the slow manifold the 1D flow obeys the differential equation

$$\dot{y}(t) = \frac{c}{bz_{,y}}\{x[y(t)] - z[y(t)]\},$$

which becomes singular at critical points defined (on the SM) by the relation

$$z_{,y} = 0. \tag{33}$$

The 3D flow (closed blue curve) follows the path $A \to B \to C \to D$. At the critical point B, the trajectory leaves the slow manifold, jumps to point C (fast stage $B \to C$), then follows the portion ($C \to D$), and finally returns to the SM in A.

Close to the critical point B, we focus on the exit of the SM. The details of our derivation is postponed to Appendix B, where we derive the normal form of the AK equations in the vicinity of B.

After rescaling the normal form (B16), we show that it takes the generic parameterless form (8), proposed as a possible description of a signal before a catastrophe [2], and displays

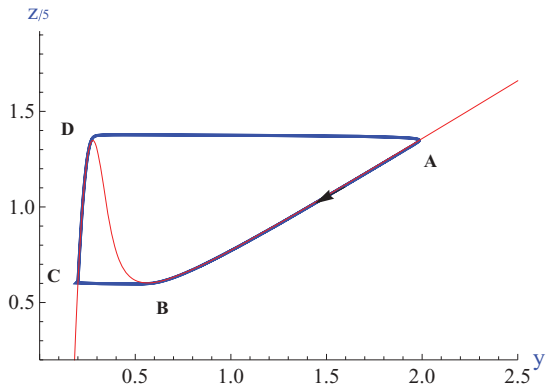

FIG. 9. (Color online) The SM trajectory $z(y)/5$ given by Eq. (32) for $a = 0.65$ and $b = 4 \times 10^{-3}$ (S-shape red curve) and the parametric plot of the 3D flow (blue curve), i.e., the numerical solution $z\{x[y(t)], y(t)\}/5$ of Eqs. (26)–(28) for $c = b/100$ and the same parameter values for a and b.

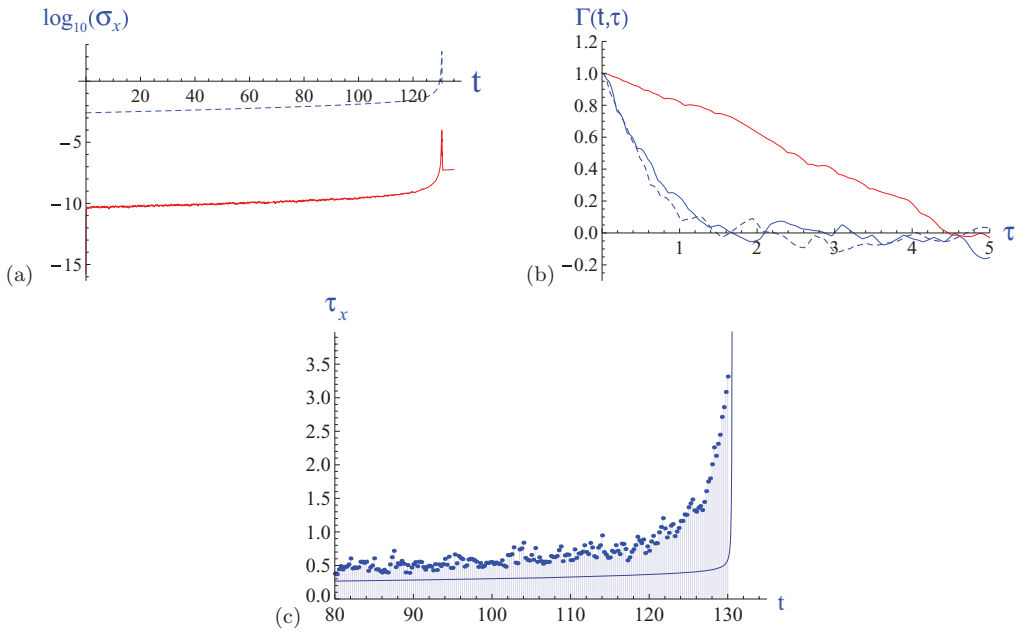

FIG. 10. (Color online) Multiplicative noise: (a) Standard deviation of the response (red solid curve) as a function of time along the path $A \to B$ before the burst, compared to $\dot{x}_0$ shifted for clarity (dashed blue curve), both on a $\log_{10}$ scale. (b) Correlation functions $\Gamma(t,\tau)$ vs τ for time values $t = 50$ (dashed), $t = 100$ (blue), and $t = 129$ (red). (c) Half-height width τ_x of the correlation function $\Gamma_{x_1}(t,\tau)$ vs time t. The input data are those of Fig. 8; noise amplitudes are $\epsilon_i = 10^{-5}$ for the three independent noise sources $f_i(t)$ $(i = x,y,z)$.

the characteristic time

$$t_0 = \left(\frac{2}{\gamma \tilde{F}_{,y^2}(x_{,y})^2}\right)^{1/3}, \tag{34}$$

where γ, $\tilde{F}_{,y^2}$, and $x_{,y}$ (taken at B) are derived in Appendix B.

As shown in Sec. III this characteristic time scale is the intermediate time scale. Expression (34) could be used to predict the burst, because the critical slowing-down effect occurs during this time interval. Finally, in terms of the AK parameters, the intermediate time scale, or precursor time, is given by the relation

$$t_0 \sim \frac{1-a}{2(\sqrt{2}\gamma)^{1/3}}, \tag{35}$$

where the parameter γ is given by (B11). For the parameter values of the above figures, we have $t_0 \sim 10$, which will be shown to agree with the precursor time deduced from the spectral analysis presented in the next section.

In summary, we have proven that the AK model, although formally different from the van der Pol model, has a normal form close to the critical point that is consistent with the dynamical saddle-mode model equation studied in [2], with an intermediate time scale given by expression (35). Consequently, as for the saddle-node model, the AK model should display a response to noise with a strong increase of the correlation time before the burst, this stage defining a precursor time of order t_0.

B. Response to noise before *B*

The response to noise of the system (26)–(28) is studied by setting $[x = x_0(t) + x_1(t),\ y(t) = y_0 + y_1(t),\ z(t) = z_0(t) + z_1(t)]$, where $x_0(t), y_0(t), z_0(t)$ is the solution of the noiseless AK equations, and the vector $V(t) = x_1(t), y_1(t), z_1(t)$ characterizes the fluctuations of the response to a noise source. These fluctuations result from the introduction of noise terms (either multiplicative or additive) in the original system. In the case of multiplicative noise sources, the response of the AK equations is a solution of the system

$$\begin{aligned}
\dot{x}(t) &= (1/b)[(1-a)x(t) - bx(t)^2 - x(t)y(t) \\
&\quad + y(t)][1 + \epsilon_x f_x(t)], \\
\dot{y}(t) &= [bx(t)^2 - x(t)y(t) - y(t) + az(t)][1 + \epsilon_y f_y(t)], \\
\dot{z}(t) &= (c/b)[x(t) - z(t)][1 + \epsilon_z f_z(t)].
\end{aligned} \tag{36}$$

We report below the result of the numerical study of this stochastic equation for small-amplitude noise. Defining the fluctuation of the response to noise by the variable $x_1(t) = x(t) - x_0(t)$, as in the previous section, we have calculated the variance, the correlation functions given by expressions (22) and (23), and the spectrum evolution along the path $A \to B$ before the burst. We found that the variance follows the evolution of the variable $\dot{x}_0(t)$, as seen in Fig. 10(a). This clearly shows that the variance growth is not a pertinent tool for predicting purposes, as already noticed in the previous section. Figure 10(b) illustrates how the correlation function changes. The striking widening of the central peak is visible on the red curve, which corresponds to time t close to the burst. A quantitative study is given in Fig. 10(c), where the half-height width of the correlation function Γ is drawn. This curve clearly shows that the widening of Γ, or increase of the correlation time of the fluctuations, occurs well before the burst, within a time interval of about $t_0 = 10$, as predicted by Eq. (35). For noise of additive type the width of the correlation function $\Gamma(t,\tau)$ behaves similarly. Moreover, as pointed out in the previous section, using the expression (23) to calculate

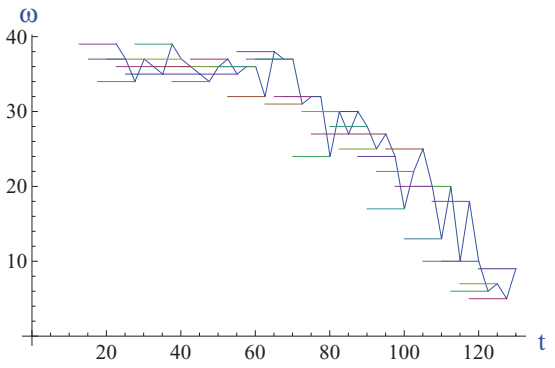

FIG. 11. (Color online) Cumulative spectral width ω of the response $x_1(t)$ to additive noise vs time before the burst. The data are the same as in other figures.

the correlation function displays an attenuated slowing-down effect, because the increase of the variance partially stifled the increase of the correlation time close to the burst; more details are given in [22]. In summary, the curve in Fig. 10(c) illustrates the main result of our study, namely, the outward sign of the critical slowing-down effect well before the catastrophe. The predictor time is shown to be of order $t_0 = 10$, in agreement with Eq. (15), which should be valid for any slow-to-fast transition of saddle-node type.

This result is also in agreement with the experimental result given in Sec. II showing a shift of the spectrum toward low frequencies before the burst. In order to compare the AK model results with the experimental ones, we have calculated the cumulative spectrum of $x_1(t)$, $C_S(t,\nu) = \int_0^\nu d\nu' S(t,\nu')$, which gives the integral over the frequency ν of the spectrum $S(t,\nu) = \langle | \int_{t-\Delta t}^{t} dt' x_1(t') \exp^{2i\pi\nu t'} |^2 \rangle$ of the fluctuations [for the response signal sampled during the time interval $(t - \Delta t, t)$], in analogy with Eqs. (2) and (3). The characteristic spectral width $\omega(t)$ defined by the relation (5) evolves in time as illustrated in Fig. 11 for the AK model with additive noise. The horizontal segments corresponding to abscissa $(t - \Delta t, t)$ have ordinates $\omega(t)$, the numerical value of the spectral width calculated during this time interval. The solid broken line joins the endpoint of each segment, in order to simulate an experimental observation of the spectrum in view of foretelling a catastrophic event [an observer cannot know $w(t)$ before time t]. The decrease of $\omega(t)$ close to the burst shows well the expected shift of the spectrum toward low frequencies, which is observed also in the experiments.

In conclusion, the AK model displays a range of parameter values where one can see the critical slowing down observed also in the experiments. We have studied the AK model for the case of small b and c parameter values, with $c \ll b$. In this case the burst occurs close to a critical point, as noticed in [4]. We have shown that close to this critical point, the 3D flow (namely, a set of three coupled ODEs) can be reduced to the two-dimensional system (B8) with "a sort of Langevin-like source" term of the form (A1) and (A2) discussed in Sec. III. The present system differs from the van der Pol equation; however, close to the critical point both models take the form of the dynamical saddle-mode model equation studied in [2].

A detailed quantitative comparison between the AK model and the creep experiment will require a more complete study, which is beyond the scope of the present work. In particular, it should be noted that including spatial variables in the AK model leads to chaotic solutions, which is in better agreement with our experiment where the limit cycle period may indeed vary by a factor of 3 from one recorded data set to another.

V. CONCLUSION

We have shown that the dynamical model of saddle-node transitions recently proposed to foretell catastrophes is applicable to describe the physics of collective dislocations. The experimental signal of the plastic deformation of the eutectic mixture of Sn-Pb subjected to a constant stress presented above clearly displays the well-known critical slowing-down effect, with a precursor time of order 1/10 of the relaxation oscillation period. This observation is shown to agree with the response to noise of a physical model proposed by Ananthakrishna and co-workers for describing creeping in ductile materials. This physical model has three parameters, and therefore it would be quasi-impossible to make a quantitative comparison between the experimental data and the theoretical model.

Here we show that the AK model has a range of parameter values for which the slow-to-fast transition is described by the dynamical saddle-node model mentioned above, which contains a time-dependant parameter hidden in the original AK equation. When adding a small noise to the AK model, we show that it indeed displays the critical slowing-down scenario. We derive the expression for the precursor time, i.e., the time during which the most intense spectral components clearly shift toward low frequencies, in terms of the three parameter values. For a given range of the parameter values we found a precursor time of order one tenth of the relaxation oscillation period, as observed in the experiment. The important result is the following: For such systems which display relaxation oscillations with saddle-node transition, we show that there exists an intermediate time scale between the slow and fast regimes, which can be used to foretell catastrophes because this time scale $t_0 = (t_{\text{creep}}/t_{\text{slip}})^{1/3}$ is much smaller than the slow time scale t_{creep} but much larger than the fast one t_{slip}. Unlike the majority of precursor tools that have focused on single-time variables, such as the probability distribution or variance, we have looked at fluctuations of the signal in the frequency domain, which means we have two-time information. These spectral precursors are prone to fewer false alarms.

APPENDIX A: SADDLE NODE

1. Local form of van der Pol–like systems

Let us sketch the normal form of van der Pol–like systems close to the jump in the spirit of Dorodnicyn's derivation. Actually we look at the formally more general situation of relaxation oscillations, namely at solutions of a set of coupled ODEs with a large parameter of the form

$$\dot{x} = \eta F(x,y) \tag{A1}$$

and

$$\dot{y} = G(x,y). \tag{A2}$$

In this set of equations dots are for time derivatives and the functions F and G are smooth with values of order 1 when

their argument is also of order one. Moreover, η is a large parameter. The slow manifold is defined by the condition that, in the large-η limit, the function $F(x,y)$ must be close to zero over at least part of the trajectory. The Cartesian equation $F(x,y)=0$ defines a curve in the (x,y) plane which allows us to find y as a function of x, at least locally. This defines the equation of motion (along the slow manifold),

$$\dot{y} = G(x(y),y),$$

where $x(y)$ is such that $F(x(y),y)=0$. The slow trajectory so defined stops at "folds" where the function $x(y)$ ceases to be well defined, namely, for values of (x,y) such that $\frac{\partial F}{\partial y} = F_{,y} = 0$, $F(x,y)=0$, and $F_{,yy}$ being not zero. This defines a discrete set of points. Near those points, the equation of motion can be solved by taking $\delta x = x - x_0$ and $\delta y = y - y_0$, where (x_0,y_0) are the Cartesian coordinates of the point 0 such that

$$F = F_{,x} = 0. \tag{A3}$$

Let us look at the solution of the coupled equations (A1) and (A2) near $O=(x_0,y_0)$. Equation (A2) is not singular at this point and so can be solved for small variation of y and for t small, such as $\delta y = tG_0$, with $t=0$ being the (arbitrary) time where the trajectory is in O and $G(x_0,y_0)=G_0$. Consider now Eq. (A1), and expand its right-hand side for δx and δy small. Because $F_{,x}=0$ at (x_0,y_0), the first nontrivial term in the Taylor expansion of F near (x_0,y_0) with respect to x is $\frac{1}{2}(F_{,xx})_0\delta x^2$. On the other hand the first term coming from the expansion with respect to δy is $F_{,y}\delta y = (F_{,y})_0 G_0 t$. Therefore, for t and δx small, the equation for δx derived from (A1) reads

$$\delta\dot{x} = \eta\left(\tfrac{1}{2}(F_{,xx})_0\delta x^2 + (F_{,y})_0 G_0 t\right), \tag{A4}$$

One can check that all terms not written explicitly there are effectively negligible compared to the ones kept. Standard rescalings allow one to transform Eq. (A4) into the "universal" equation (8), provided various constraints of sign are satisfied by the quantities $F_{,xx}$, $F_{,y}$, and G all computed at (x_0,y_0).

2. Explicit solution of the generic equation (8)

Note that the notation $x(t)$ in Sec. III stands for any function which is locally described by Eq. (8). In our paper $x(t)$ stands for the elongation rate of the creeping process. The addition of the quartic term in the potential in Sec. III B is valid for the case of gradient flow dynamics, and therefore it is formally not applicable to the cases where the local equation (8) describes a slow-to-fast transition in a limit cycle. However, since we are interested in the behavior of the solution before and at the instant of the jump, we use the gradient flow description because it allows us to suppress the divergence of Eq. (8) at t_c. The reader should not be confused by the fact that the quartic potential solution better behaves after t_c as the elongation [$\ell(t)$ in the experiment and in the AK model], since both the elongation and the elongation rate reduce to the same generic equation (8) after appropriate rescaling.

We look at the solution of Eq. (8) transiting from the "stable" fixed point at "large" negative times to the rolling down toward positive value of x at positive times. This solution behaves like $x(t) \approx -\sqrt{-t}$ at large negative times. Equation (8) is of the Riccati type and can be integrated by introducing the function $u(t)$ such that $x(t) = -\frac{\dot{u}}{u}$, where $\dot{u} = \frac{du}{dt}$ and $u(t)$ is a solution of Airy's equation [20] $\ddot{u} + tu = 0$.

In terms of the variable $u(t)$ the solution of Eq. (8) relevant with the boundary conditions is the Airy function $Ai(-t)$, which can be written as

$$U(t) = Ai(-t) = \int_0^{+\infty} \cos\left(\frac{u^3}{3} - ut\right) du.$$

Yet we have only solved the transient problem near the saddle-node bifurcation.

a. Close to t_c

The transition ends when t becomes equal to the first zero of the Airy function $Ai(-t)$, i.e., the smallest root of the equation $U(t)=0$, a pure number, at about $t_c \approx 2.338$. This corresponds to a divergence of $x(t) = -\frac{\dot{u}}{u}$, which behaves as

$$x(t) \approx \frac{1}{t_c - t} - \frac{t_c}{3}(t_c - t) + \cdots \tag{A5}$$

just before this transition, as derived by expanding $U(t)$ close to t_c.

Therefore the "generic" equation (8) for the dynamical saddle-node bifurcation displays a finite-time singularity. Let us elaborate upon the following mathematical subtlety. This property of the *local flow*, which results from the folding of the slow manifold, differs qualitatively from the finite-time singularity found in the Dieterich-Ruina equations [10], where it was a property of the flow *reduced to the slow manifold* which is everywhere convex, as discussed in Sec. I. In the case of the dynamical saddle-node bifurcation the singularity requires one to consider the dynamics both on and off the slow manifold, and this happens because the geometry forbids the continuation of an exact trajectory on this folded slow manifold.

b. Variance of $x_1(t)$

To make the developments above more concrete, let us consider delta-correlated (or white) noise, such that $\langle \xi(t_a)\xi(t_b)\rangle = \delta(t_a - t_b)$.

The pair correlation of $x_1(t)$ is given by

$$\langle x_1(t)x_1(t')\rangle = \frac{1}{U^2(t)U^2(t')}\int_{-\infty}^{\inf(t,t')} d\tilde{t}\,U^4(\tilde{t}),$$

where $\inf(t,t')$ is the smallest of the two real numbers t and t'. The behavior of this pair correlation for large negative values of both t and t' is derived from the asymptotic expression of Airy's function, $Ai(-t) \approx \frac{e^{-\frac{2}{3}(-t)^{3/2}}}{2\sqrt{\pi}(-t)^{1/4}}$. By setting $\tau = \frac{\tilde{t}}{t}$ and $F(\tau) = 1 - \tau^{3/2}$, the variance of the fluctuations can be written as $\langle x_1(t)^2\rangle \approx (-t)\int_1^{\infty}\frac{d\tau}{\tau} e^{\frac{8}{3}(-t)^{3/2}F(\tau)}$.

In the limit $(-t)\to\infty$ the integral is concentrated near $\tau = 1$ so that

$$\langle x_1(t)^2\rangle \approx \tfrac{1}{4}(-t)^{-\frac{1}{2}}, \tag{A6}$$

which shows that the variance increases as time goes on.

3. Short time scale

We show that the short time $t_{\rm slip}$ of our model equation (14) is of order unity, by matching the solution $X(T)$ of the

universal equation to the solution of Eq. (A7) below, in the vicinity of the critical point

$$t_c(a) = a^{-1/3} t_c,$$

where $t_c \sim 2.338$ is the first zero of the Airy function, as defined in Appendix A 2. Because $X(T)$ behaves like $\frac{1}{t_c - T}$ before it diverges, it follows that the solution $x(t)$ behaves as $\approx \frac{1}{a^{-1/3} t_c - t}$ for "large" values of $\delta t = a^{-1/3} t_c - t$ before the critical time. This becomes of order one when δt becomes also of order one. When this happens, the term at in Eq. (14) is negligible, and therefore the solution of this equation, which can be matched with the solution near the bifurcation, is the solution of the integrable equation

$$\dot{x} = x^2 - x^3, \tag{A7}$$

with the asymptotic behavior for very large negative times $x(\delta t) \sim -\frac{1}{\delta t}$. This equation shows that, in our model, the fast time scale is of order one, because it has no explicit dependence with respect to the small parameter a.

APPENDIX B: AK MODEL CLOSE TO THE JUMP

1. Stability of the 3D flow

We consider the linear stability of 3D flow, with special focus on the first stage described in Sec. IV, which precedes the fast jump. In the slow regime, under the assumption of a 3D flow of the form $x(t) = x_0(t) + \delta x \exp \lambda t$ [and similar expressions for $y(t)$ and $z(t)$] close to the trajectory $x_0(t), y_0(t), z_0(t)$, the exponents λ are the eigenvalues of the Jacobian matrix

$$\begin{pmatrix} (1 - a - 2bx_0 - y_0)/b & (1 - x_0)/b & 0 \\ 2bx_0 - y_0 & -(x_0 + 1) & a \\ c/b & 0 & -c/b \end{pmatrix}, \tag{B1}$$

or solutions of the equation

$$\lambda^3 + a_2 \lambda^2 + a_1 \lambda + a_0 = 0, \tag{B2}$$

with $a_2 = [c - (1 - a - y_0)]/b + 3x_0 + 1$, $a_1 = [2x_0 + (y_0 + a - 1)/b](x_0 + 1 + c/b) + (x_0 + 1)c/b - (x_0 - 1)(y_0 - 2bx_0)/b$, and $a_0 = -c(1 + x_0)(2bx_0 + y_0 + a - 1) - (y_0 - 2bx_0)(x_0 - 1) + a(x - 0 - 1)/b^2$.

As illustrated in Fig. 10 of our paper [22], one of the eigenvalues is real and negative all along the trajectory, while the other two become complex conjugates in the slow regime, their real part crossing zero before the burst at time $t_{\mathrm{lyap}} \sim t_c - 3$. The time interval $t_c - t_{\mathrm{lyap}}$ depends on the values of the parameters a, b, and c. It is generally a small fraction of the limit cycle period. Here we find that the numerical value of $t_c - t_{\mathrm{lyap}}$ is nearly equal to the intermediate time scale t_0 for the model, derived in the next Appendix.

2. Local form close to B

The coordinates of the critical point B in phase space x, y, z are solutions of Eqs. (31) and (33). From Eq. (31) we derive the following expression for $x_{,y} = \frac{\partial x}{\partial y}$:

$$x_{,y} = -\frac{(x - 1)^2}{1 - a + bx^2 - 2bx}, \tag{B3}$$

which should be identical to the expression of $x_{,y}$ taken from the relation (33),

$$(x_{,y})_B = \frac{x^2 - 1}{3bx^2 - (2b + 1 - a)x}. \tag{B4}$$

These two expressions are identical if x_B is a root of the cubic polynomial equation

$$x(x - 1)(1 + 2\tilde{b} - 3\tilde{b}x) = (x + 1)(1 - 2\tilde{b}x + \tilde{b}x^2), \tag{B5}$$

where $\tilde{b} = b/(1 - a)$. The positive solution x_B and the corresponding value of $y_B = [(1 - a)x_B - bx_B^2]/(x_B - 1)$ and z_B satisfying Eqs. (31) and (32), respectively, are given at leading order with respect to the small parameter $\tilde{b}$ by

$$\begin{aligned} x_B &= \sqrt{2} + 1 + \frac{8 + 5\sqrt{2}}{2} \frac{b}{1 - a}, \\ y_B &= (1 - a)(1 + \sqrt{2}) - \frac{8 + 11\sqrt{2}}{2} \frac{b}{1 - a}, \\ z_B &= \frac{(3 + 2\sqrt{2})(1 - a)}{a} - b \frac{10 + 7\sqrt{2}}{a}, \end{aligned} \tag{B6}$$

valid in the parameter range $b \ll (1 - a)$.

We next derive the normal form describing the dynamical behavior of the solution close to the critical point. By assuming that the variable x follows adiabatically the variable y according to Eq. (31), the original system reduces to

$$\dot{y} = F(y, z), \quad \dot{z} = \frac{c}{b}[x(y) - z], \tag{B7}$$

defining the dynamics for the portion of the trajectory near B, including the burst $B \to C$. This is confirmed by the numerics: starting from the point B, with numerical initial conditions (B6), the behavior of the solutions of Eq. (B7) agree well with the 3D flow (see Fig. 11 of [22]).

Since we are interested in the description of the solution before and at the burst, in the intermediate regime where x remains close to x_B, we shall pursue our analysis by canceling the terms bx^2 in (31) and in F, because $bx_B \ll 1$. This leads to the system

$$\begin{aligned} x &= \frac{y}{y - 1 + a}, \\ \dot{y} &= \tilde{F}(y, z), \\ \dot{z} &= \frac{c}{b}[x(y) - z], \end{aligned} \tag{B8}$$

where $\tilde{F} = -xy - y + az$. Close to B and during the burst, the variable z is essentially constant, due to the small value of the ratio c/b, whereas the variable y jumps toward smaller values, as shown in Fig. 12 of Ref. [22]. Therefore at leading order with respect to the small parameter c/b, the solution of the second of Eqs. (B7) is given by

$$z(t) = z_B + \frac{c}{b}(x_B - z_B)t \tag{B9}$$

in the vicinity of B. By inserting this local solution (B9) for $z(t)$ into the system (B8), the exit from the SM is then described by a single equation for the local variation $\delta y = y - y_B$ of y of the variable y, which is of the form

$$\delta \dot{y} = \sum_{n>2} \frac{1}{n!} (\tilde{F}_{,y^n})_B \delta y^n + \gamma \delta t, \tag{B10}$$

where

$$\gamma = (ac/b)(x_B - z_B), \tag{B11}$$

and $\tilde{F}_B^{(n)}$ sets for the nth derivative of $\tilde{F}$ with respect to the variable y, taken at point B [and note that $(F_{,y})_B = 0$ at the critical point B]. Using the reduced system (B8), for the first two derivatives of $\tilde{F}$ with respect to y we write

$$\begin{aligned} \tilde{F}_{,y^2} &= -yx_{,y^2} - 2x_{,y}, \\ \tilde{F}_{,y^3} &= -yx_{,y^3} - 3x_{,y^2}. \end{aligned} \tag{B12}$$

Expanding all expressions close to B at leading order with respect to the small parameter b, one obtains

$$\begin{aligned} (x_{,y})_B &= -\frac{2}{1-a}, \\ (x_{,y^2})_B &= -\frac{4\sqrt{2}}{(1-a)^2}, \\ (\tilde{F}_{,y^2})_B &= -\frac{4\sqrt{2}}{1-a}, \\ (\tilde{F}_{,y^3})_B &= \frac{24}{(1-a)^2}. \end{aligned} \tag{B13}$$

At this stage we can limit the series expansion in Eq. (B10). A rough approximation for the series to converge is given by $(\tilde{F}_{,y^3})_B \delta y < 3(\tilde{F}_{,y^2})_B$. Using expressions (B13) and the first of Eqs. (B8) gives the range of variation

$$|\delta y| < \frac{3}{\sqrt{2}}(1-a), \quad |\delta x| < \sqrt{2}. \tag{B14}$$

In this range the local form of the AK equations close to B becomes

$$\delta\dot{y} = \tfrac{1}{2}(\tilde{F}_{,y^2})_B \delta y^2 + \gamma\delta t, \tag{B15}$$

or in terms of the variable $x(t)$,

$$\delta\dot{x} = (x_{,y})_B \left[\tfrac{1}{2}(\tilde{F}_{,y^2})_B \delta y^2 + \gamma\delta t\right], \tag{B16}$$

which is identical to Eq. (A4). Finally, by setting

$$T = \left[\frac{-\gamma(x_{,y})_B^2(\tilde{F}_{,y^2})_B}{2}\right]^{1/3} \delta t, \tag{B17}$$

and $X = [\frac{(x_{,y})_B(\tilde{F}_{,y^2})_B)^2}{4\gamma}]^{1/3}\delta x$, the relation (B16) takes the generic form (8) without any parameter, recently proposed as a possible description of a signal before a catastrophe. The time scale deduced from Eq. (B17) is the intermediate time scale (15).

[1] G. Ananthakrishna, Phys. Rep. **440**, 113 (2007).

[2] Y. Pomeau and M. Le Berre, arXiv:1102.5637; Y. Pomeau, M. Le Berre, J.-L. Le Mouël, C. Narteau, and P. Fromy, *Comptes-rendus de la 14e Rencontre du Non Linéaire*, edited by C. Josserand, M. Lefranc, and C. Letellier (Non-Linéaire, Saint-Etienne du Rouvray, 2011).

[3] G. Ananthakrishna and D. Sahoo, J. Phys. D **14**, 2081 (1981).

[4] M. C. Valsakumar and G. Ananthakrishna, J. Phys. D **16**, 1055 (1983).

[5] A. A. Dorodnicyn, Am. Math. Soc. Transl. Seri. One **4**, 1 (1953) [translated from Priklad Mat. Mek. **11**, 313 (1947)].

[6] V. A. Dubrovskiy and V. N. Sergeev, GEOS, Moscow **1**, 222 (2001) (in Russian); Dok. Phys. **49**, 231 (2004).

[7] V. A. Dubrovskiy and V. N. Sergeev, Ital. J. Eng. Geol. Environ., Spec. Issue **1**, 183 (2006).

[8] D. Sornette and J. V. Andersen, Europhys. Lett. **74**, 778 (2006).

[9] Y. Haung, H. Salem, C. Sammis, and D. Sornette, Europhys. Lett. **41**, 43 (1994); C. G. Bufe and D. J. Varnes, J. Geophys. Res. **98**, 9871 (1990); A. Guarino, S. Ciliberto, A. Garcimartín, M. Zei, and R. Scorretti, Eur. Phys. J. B **26**, 141 (2002); R. De and G. Ananthakrishna, Europhys. Lett. **66**, 715 (2004); see Nature Debates (1999) http://helix.nature.com/debates/earthquake.

[10] Y. Pomeau and M. Le Berre, in *Chaos, CNN, Memristors and Beyond*, edited by A. Adamatzky and G. Chen (World Scientific, Singapore, 2012) (to be published); see also Y. Pomeau and M. Le Berre, arXiv:1107.3331.

[11] In situations similar to one of the van der Pol equation in the limit of large nonlinearities, the slow to fast transition occurs at the point on the slow manifold where the large component of the velocity is tangent to the slow manifold. This tangency never happens in the Dieterich-Ruina equations because, there, the large component of the velocity crosses everywhere the slow manifold at a finite angle. Therefore the scenario of slow to fast transition is different in the Dieterich-Ruina equations than what it is in limit cycles of the Liénard–van der Pol–like equations.

[12] This product came from Tel-Atomic, Inc., a company that specializes in "Tools for Teaching Advanced Physics." It is no longer available as a commercial product. One reason this instrument is no longer manufactured was the loss, due to a factory fire, of readily available chips that constituted the key component (NE5521n integrated circuit) used in the support electronics for its displacement sensor [13]. The same first example of fully differential capacitive sensors is also employed (except employed as a pair, for mechanical common mode rejection of noise) with different electronics, in another of the company's instruments, the computerized Cavendish balance [14].

[13] US Patent No. 5461319 (1995). A description of the sensor is provided at http://telatomic.com/mechanics/sensor.html.

[14] http://telatomic.com/mechanics/cavendish-balance.html. The support electronics for this balance employs a novel capacitive to digital converter (AD7745), which was marketed by Analog Devices soon after the demise of the NE5521n.

[15] The USB4CH is described online at http://www.symres.com.

[16] The VolksMeter is described online at http://psn.quake.net/volksmeter/State-of-the-art-Digital-Seismograph.pdf.

[17] The Earthquake data are shown at http://physics.mercer.edu/hpage/CSP/bounce.html.

[18] R. Thom, *Stabilité structurelle et morphogénese* (Benjamin, New York, 1972); V. I. Arnol'd, *Catastrophe Theory*, 3rd ed. (Springer-Verlag, New York, 1992).

[19] Sweeping bifurcation in dynamical systems has been studied before. To the best of our knowledge it has been considered in

continuous transitions in the following two cases: first, from the point of view of bifurcation theory with a time direction inverse of ours, namely in the direction where a pair of equilibria appears in forward time; see T. Erneux and P. Mandel, SIAM J Appl. Math. **46**, 1 (1986); second, for continuous thermodynamical phase transitions; see D. Sornette, J. Phys. I (France) **4**, 209 (1994). J.-P. Bouchaud and R. Cont, Eur. Phys. J. B **6**, 543 (1998), also studied the saddle-node transition with noise, considering the bifurcation for different shapes of potential near the transition value. They suggest a change of shape of potential resulting from the time dependence of a control parameter. However they do not solve the dynamical problem with an *explicitly* time-dependent potential, whereas this is the key of our study. We show in particular that the slow dependence (with respect to time) of the potential allows one to obtain a universal picture of the dynamical saddle-node bifurcation with an intermediate time scale near the transition which could precisely be seen as a precursor time, a time scale absent in this reference.

[20] M. Abramowitz and I. A. Stegun, eds., *Handbook of Mathematical Functions with Formulas, Graphs, and Mathematical Tables* (Dover, New York, 1965), Chap. 10.

[21] C. Kuehn, Physica D **240**, 1020 (2011), and references herein.

[22] R. D. Peters, M. Le Berre, and Y. Pomeau, arXiv:1204.1551.